Supporting Information to

Strong light-field driven nanolasers

Richard Hollinger[†,‡], Pavel Malevich[§], Valentina Shumakova[§], Skirmantas Ališauskas[§,$], Maximilian Zapf [‖], Robert Röder[‖], Audrius Pugžlys[§], Andrius Baltuška[§], Carsten Ronning[‖,#], Christian Spielmann[†,‡,#], Daniil Kartashov[†,#,]*

[†]Institute of Optics and Quantum Electronics, Friedrich-Schiller University Jena, Max-Wien-Platz 1, 07743 Jena, Germany.

[‡]Helmholtz-Institut Jena, Helmholtzweg 4, 07743 Jena, Germany.

[§]Institute for Photonics, Vienna University of Technology, Gußhausstrasse. 25-29, 1040 Vienna, Austria.

[‖]Institute of Solid State Physics, Friedrich-Schiller University Jena, Max-Wien-Platz 1, 07743 Jena, Germany.

[#]Abbe Center of Photonics, Albert-Einstein-Straße 6, 07745 Jena, Germany.

E-mail: daniil.kartashov@uni-jena.de, carsten.ronning@uni-jena.de

Nanowire growth and sample preparation

A scanning electron microscope (SEM) image of the disordered NW array used in the experiments is shown in Fig. S1. The diameter and the length of the nanowires are 200-250 nm and 5-10 μm, respectively. The batches of single crystalline, wurtzite ZnO nanowires were synthesized using a simple vapor-phase-transport (VPT) technique in a horizontal tube furnace[1]. For the synthesis of the disordered batches, the vapor-liquid-solid (VLS) mechanism was enabled[2]. Briefly, approximately 1g of ZnO powder was used as a source material. Silicon chips with a 10 nm thin Au layer on the top were used as growth substrates. The ZnO powder was heated to 1350 °C and the pressure was kept constant at 100 mbar. A flow of 50 sccm Ar gas carried the ZnO vapor towards the growth substrates for a growth time of 1 hour. During the growth process the Au layer melts and forms catalyst droplets acting as nucleation sites. Therefore, the nanowires grow without preferential alignment. The dimensions and morphology of the nanowire arrays were determined with a FEI Helios 600 SEM/FIB system with a lateral resolution of about 1 nm.

Single nanowires were transferred to clean SiO_2/Si (1.5 μm of SiO_2 on top) substrates using a dry imprint method: pressing the sample face-to-face. The substrates had a lithographically imprinted coordinate system. Thus, using an optical imaging system (see below), it was possible to locate the transferred well-separated individual nanowires laying at the surface of the substrate and address them in different optical systems.

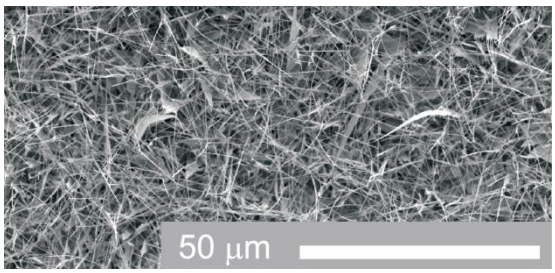

Figure S1. *SEM-image of a randomly oriented ZnO nanowire array grown by a simple vapor transport method via the VLS mechanism.*

Laser systems

The experiments at 0.8 μm were carried out by using 35 fs laser pulses from a Ti:Saphire amplifier system operating at 1 kHz repetition rate and generating pulses with energies up to 0.8 mJ. For calibration of the intensity on the target, the pulse duration was measured using an interferometric autocorrelator (Femtolasers Femtometer) as the spatial distribution of the intensity in the focus was recorded with a CCD-camera (ThorLabs BC106N-VIS).

Mid-IR 0.1 mJ, 100 fs laser pulses at a repetition rate of 500 Hz were generated in a 3-stage optical parametrical amplifier (OPA) based on type II potassium titanyl arsenate (KTA) nonlinear optical crystals. The white light seeded OPA was pumped by 8.5 mJ, 200 fs pulses originating from Yb:CaF_2 regenerative amplifier operating at 1030 nm central wavelength.

Generated in the OPA signal and idler pulses are tunable in the spectral range of 1.4-2.06 μm and 2.06-4.0 μm respectively. The idler pulses, which are slightly negatively chirped, were compressed to ~100 fs duration by inserting into the beam different amount of silicon plates, possessing positive dispersion in this spectral range. Temporal and spatial characterization of the mid-IR laser pulses was performed by using second-harmonic-generation frequency resolved optical gating (SH-FROG) and knife edge methods, respectively.

In all experiments the intensity on the target was calculated from the measured pulse energy, temporal pulse profile and spatial intensity distribution on the sample.

μ-Photoluminescence setup for single wire experiments

Figure S2 shows the μ-photoluminescence setup used for monitoring of spontaneous emission and lasing from a single nanowire. The femtosecond laser pulse energy was set with a wire grid (WG) polarizer. The pump beam was focused with a CaF_2 lens with a focal length of f = 10 cm under an angle of 45° to the normal of the substrate. The emission from a nanowire was detected perpendicular to the wires using a 100x objective with a 0.4 NA (MO) and reimaged to the entrance slit of an imaging spectrometer (Andor Shamrock 193i) equipped with a Peltier-cooled CCD (Andor Newton DU920P BR-DD). For the purpose of orientation on the SiO_2/Si marker, a nanowire could be irradiated with a white light source and imaged to a CCD camera with the same objective and a lens when the collected radiation was redirected by a flip mirror to the CCD-camera. A band-pass filter (BP) was used to filter out the pump wavelength.

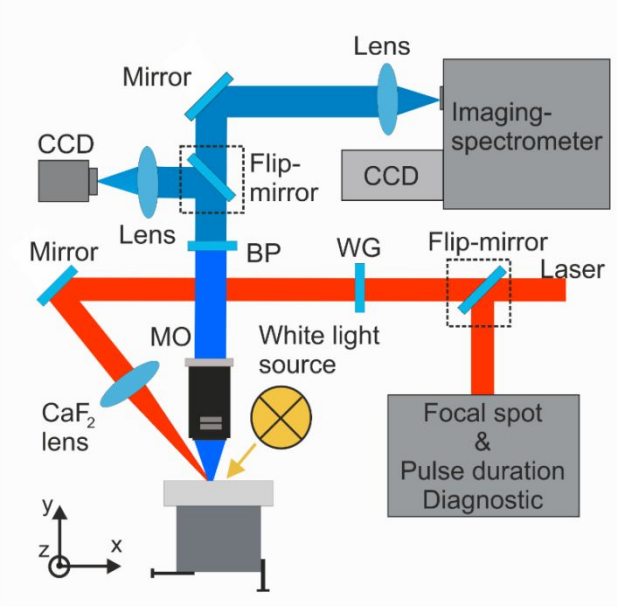

Figure S2. *μ-Photoluminescence setup to investigate the dependence of the emission from a single ZnO NW on the pump power. MO is a microscope objective, WG is a wire-grid polarizer, and BP-a band-pass filter.*

Lasing in CdS nanowires

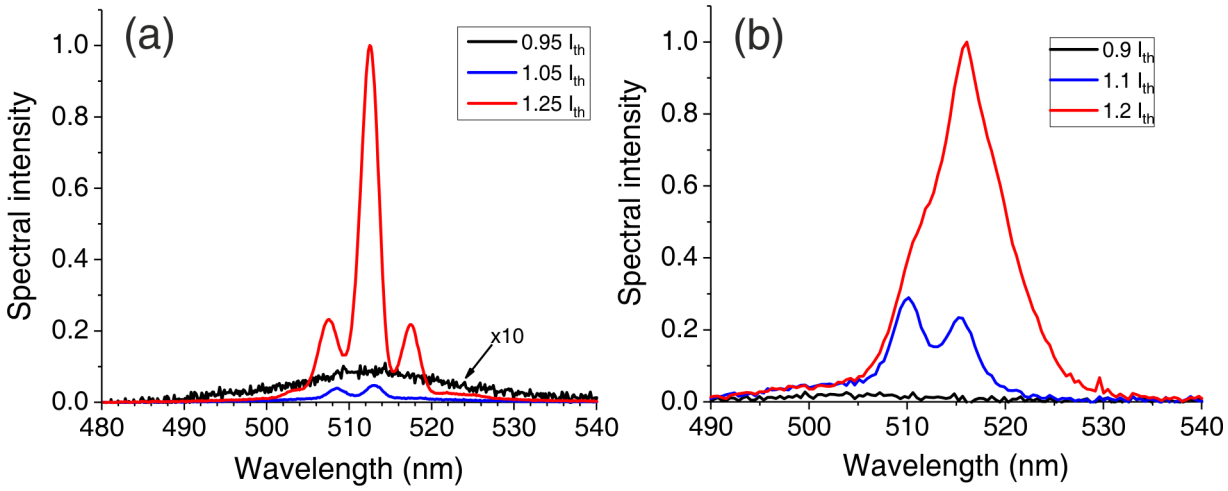

Figure S3. *Emission spectrum from a single CdS nanowire pumped by a) 35 fs pulses at 0.8 μm wavelength (two-photon absorption) and b) 105 fs pulses at 3.5 μm wavelength (tunnel excitation). Note that the intensity of the spontaneous emission in a) is multiplied by a factor of 10 to improve the visibility.*

Optical setup to determine the wavelength dependent lasing threshold

Figure S3 illustrates the optical setup used for determination of the dependence of the lasing threshold on the pump wavelength from disordered ZnO nanowire arrays. The intensity of the pump was controlled by a wire-grid polarizer (WG) and the pump beam was focused onto the randomly oriented NW array using a CaF_2 lens. The emission from the array was collected under an angle of 45° with a 4x microscope objective (MO, 0.15 NA) and imaged with a lens to the entrance slit of a spectrometer (Ocean Optics USB400 UV-VIS). A band-pass filter (BP) was used to block the reflected pump wavelength. To calculate the threshold pumping intensity spatial beam profile on the target was measured using the knife-edge scan method for every wavelength; the pulse duration was measured by using SHG-FROG method. The pulse duration and the focal spot size of 0.8 μm pumping beam was 30 fs and 600 μm respectively and varied within the range 105-130 fs and 100-200 μm with tuning of the wavelength in the spectral range 1.5-4 μm.

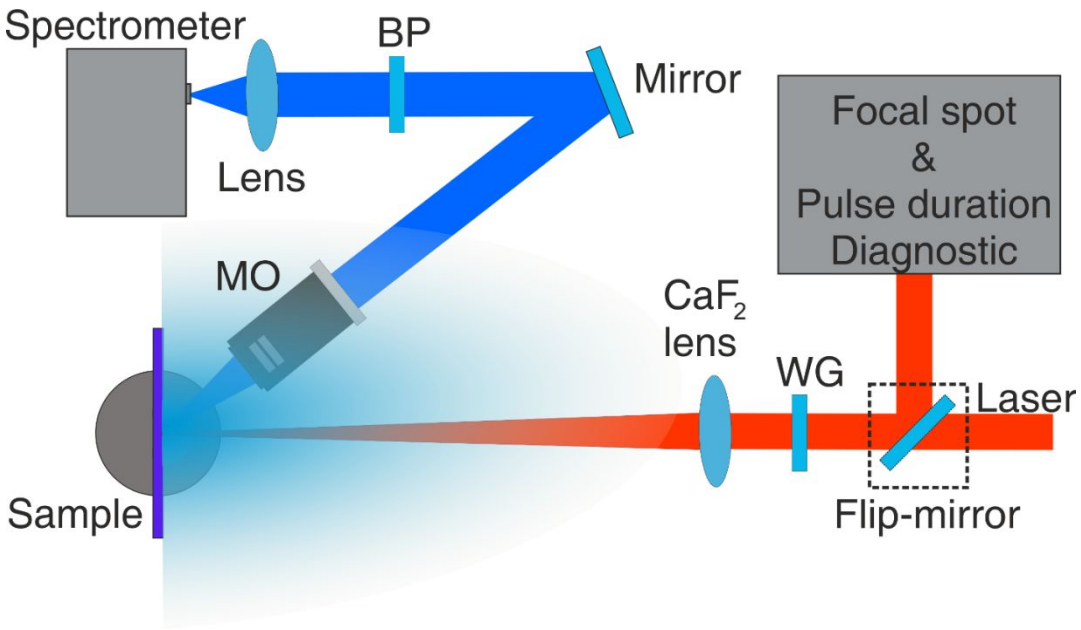

Figure S4. *Experimental setup used to investigate the wavelength dependence of the laser threshold in the disordered NW arrays. MO is a microscope objective, WG is a wire-grid polarizer, and BP-a band-pass filter.*

Measurements with different pump spot sizes for a pumping wavelength of 0.8 □m are displayed in Figure S5. The almost constant threshold as a function of spot size indicates that lasing observed in our experiments is unlikely due to random lasing, as the threshold should decrease with increasing spot size for such a scenario.

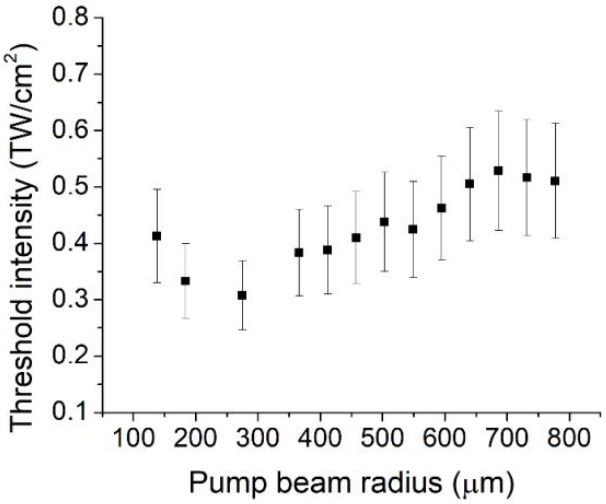

Figure S5*. Threshold intensity as a function of excitation spot size while pumping a ZnO nanowire array with a wavelength of 800 nm.*

Theoretical model of strong field excitation in semiconductors

As a result of the absorption of multiple photons from the pumping pulse or tunneling the electrons excited from the VB to the CB, the excited electrons might possess an excessive energy relative to the bottom of the CB. For example, pumping via three-photon absorption at 0.8 μm (the energy of the quanta ≈1.55 eV) in ZnO would result in 1.28 eV excessive energy of the excited electrons. This energy will be relaxed in electron-phonon collisions on a picosecond time scale resulting in a distribution of electrons near the bottom of the CB. Additionally, free electrons in the CB might also absorb energy during the pumping time from the pump pulse via the inverse bremsstrahlung mechanism or free carrier absorption[3] (FCA). When the electrons are hot enough that their kinetic energy is above a certain threshold value E_c, they can excite further electrons from the VB to the CB via electron by impact ionization/excitation. Therefore, we describe the population in the CB by two fraction of electrons, the hot fraction n_{hot} and the cold fraction n_e, related by the following rate equations:

$$\frac{dn_{hot}}{dt} = w_K(I(t),\omega) - \frac{n_{hot}}{\tau_C} + \frac{\sigma(\omega,n_{hot})}{E_C} n_{hot} I(t) \qquad (1)$$

$$\frac{dn_e}{dt} = \frac{n_{hot}}{\tau_C} - \frac{n_e}{\tau_e} \qquad (2)$$

Here the strong field excitation rate $w_K(I,\omega)$ is calculated using the Keldysh expression[4] $w_k = 2\frac{2\omega}{9\pi}\left(\frac{m^*\omega}{\hbar\sqrt{\gamma}}\right)^{\frac{3}{2}} Q\left(\gamma,\frac{\Delta_{NP}}{\hbar\omega}\right) \times \exp\left[-\pi\left\langle\frac{\Delta_{NP}}{\hbar\omega}+1\right\rangle\frac{\mathcal{K}(\phi)-\mathcal{E}(\phi)}{\mathcal{E}(\Theta)}\right]$, where $Q(\gamma,x) = \sqrt{\frac{\pi}{2\mathcal{K}(\Theta)}} \times \sum_{n=0}^{\infty}\exp\left[-\pi\cdot\frac{\mathcal{K}(\phi)-\mathcal{E}(\phi)}{\mathcal{E}(\Theta)}\cdot n\right]\cdot\Phi\left[\sqrt{\frac{\pi(2\langle x+1\rangle-2x+n)}{2\cdot\mathcal{K}(\Theta)\cdot\mathcal{E}(\Theta)}}\right]$, $\mathcal{K}$ and $\mathcal{E}$ are complete elliptic integrals, $\Theta = \frac{1}{1+\gamma^2}$ and $\phi = \frac{\gamma^2}{1+\gamma^2}$, $\gamma = \frac{\omega\sqrt{m^*\Delta}}{eF}$ is the Keldysh parameter, $\Phi(x) = \int_0^x \exp\left(\xi^2 - x^2\right)d\xi$ is the Dawson integral, Δ is the intrinsic band gap, m^* is the effective electron mass, ω is the laser frequency, e is the elementary charge and F is the amplitude of the electric field in the laser pulse related to the laser pulse intensity $F(t) = \sqrt{2I(t)/\varepsilon_0 c}$, c and ε_0 denote the vacuum velocity of light and permittivity, $\Delta_{eff} = \frac{2}{\pi}\Delta\left[\frac{\sqrt{1+\gamma^2}}{\gamma^2}\cdot E(\Theta)\right]$ is the bandgap value modified due to the Stark shift.

The second term in Eq. (1) describes the thermalization of the hot excited electrons with a single exponential decay rate $1/\tau_c$ due to electron-phonon scattering. The third term describes the growth in the hot electron population due to free-carrier absorption (FCA) and electron impact excitation from the VB. This is, in fact, the term which is responsible for the avalanche ionization in the material. The conductivity $\sigma(\omega,n_{hot}) = \frac{e^2}{m_e\varepsilon_0 c\,\gamma_e(n_{hot})}\left(1+\frac{\omega^2}{\gamma_e(n_{hot})^2}\right)^{-1}$ was calculated using the Drude model with the density dependent electron scattering rate γ_e calculated from the empirical formula presented in Ref. *(5)* with material parameters for ZnO given in Ref. *(6)*. In simulations without FCA $\sigma(\omega,n_{hot})$ was set to 0.

Equation (2) describes the balance in the population of cold electrons governed by the $1/\tau_c$ cooling rate of the hot electrons and by the spontaneous radiative decay rate $1/\tau_e$.

Simulations shown in Fig. 4 of the manuscript are carried out assuming a Gaussian shape of the laser pulse intensity $I(t) = I_0 \cdot \exp\left[-4\ln(2)\frac{t^2}{\tau_{FWHM}^2}\right]$ with the experimentally measured values of the pulse duration and the peak intensity I_0. Other model parameters are $\tau_C = 1$ ps[7,8] and $\tau_e = 100$ ps[9]. The intrinsic band gap Δ has a value between 2.9 - 3.37 eV dependent on the excited carrier density and model describing band gap renormalization[10]. The effective mass m_e in the range between 0.14 - 0.5 m_0 depends on the excited carrier density, assumed non-parabolicity of the conduction band and orientation of the pump pulse electric field in respect to the nanowire c-axis, here m_0 depict the electron rest mass[11-13]. The critical energy E_C has to be larger than the modified band gap Δ_{eff} and can be up to $1.5\Delta_{eff}$ (Ref. 3). The ratio $\frac{\sigma}{E_C}$ in equation 1 is in the order of 10^{-4} and consistent with numbers used to scale free carrier absorption in ZnO nanorods[14]. In our simulations the carrier density dependent BGR model suggested in Ref. 15 , an effective mass of 0.29 m_0 and a value for E_C of $1.3\Delta_{eff}$ were used.

The rate equation system (1)-(2) contains three significantly different time scales. In fact, Eq. (1) describes the dynamics of the population of the hot electron fraction on a fs-time scale of the pump pulse, which is much shorter than the intra-band relaxation time scale τ_C. Thus, the cold electron fraction remains negligible on the time scale of the material interaction with the pump pulse. Then the hot electron fraction relaxes to the cold one on a picosecond time scale, which is much shorter than the radiative spontaneous decay time τ_e. Therefore, the pump threshold intensity is determined by the condition that the maximal excited carrier density n_e reaches a number of $2\cdot10^{19}$ cm^{-3}, the value derived in Ref.16 and enabling a negative absorption (gain).

References

(1) Borchers, C.; Müller, S.; Stichtenoth, D.; Schwen, D.; Ronning, C. *Journ. Phys. Chem. B* **2006**, *110*, 1656-1660.

(2) Wagner, R. S.; Ellis, W. C. *Appl. Phys. Lett.* **1964**, *4*, 89-90.

(3) Ristau, D. *Laser-induced damage in optical materials*, CRC Press: Boca Raton, 2015.

(4) Keldysh, L. V. *Sov. Phys. JETP* **1965**, *20*, 1307-1314.

(5) Masseti, G.; Severi M.; Somi, S. *IEEE Trans. Electr. Dev.* **1983**, *30*, 764-769.

(6) Ellmer, K. *Journ. Phys. D* **2001**, *34*, 3097-3108.

(7) Song, J. K.; Szarko, J. M.; Leone, S. R.; Li, S.; Zhao, Y. *Phys. Chem. B* **2005**, *109*, 15749-15753.

(8) Song, J. K.; Willer, U.; Szarko, J. M.; Leone, S. R.; Li, S.; Zhao, Y. *Phys. Chem. C* **2008**, *112*, 1679-1684.

(9) Wille, M.; Sturm, C.; Michalsky, T.; Röder, R.; Ronning, C.; Schmidt-Grund, R.; Grundmann, M. *Nanotech*. **2016**, *27*, 225702-1 - 225702-7.

(10) Versteegh, M. A. M.; T. Kuis, T.; Stoof, H. T. C.; Dijkhuis, J. I. *Phys. Rev. B* **2011**, *84*, 035207-1 - 035207-19.

(11) Schleife, A.; Fuchs, F.; Rödl, C.; Furthmüller, J.; Bechstedt, F. *Phys. Stat. Solidi B* **2009**, *246*, 2150-2153.

(12) Morkoç, H.; Özgür, Ü. *Zinc Oxide: Fundamentals, Materials and Device Technology*, Wiley-VCH: Weinheim, 2009.

(13) Ellmer, K.; Klein, A.; Rech, B. *Transparent Conductive Zinc Oxide: Basics and Applications in Thin Film Solar Cells*, Springer: 2008.

(14) Hyyti, J.; Perestjuk, M.; Mahler, F.; Grunwald, R.; Güell, F.; Gray, C.; McGlynn, E.; Steinmeyer, G. *Journ. Phys. D* **2018**, *51*, 105306.

(15) Bànyai, L.; Koch, S. W. *Zeit. für Phys. B* **1986**, *63*, 283-291.

(16) Nakamura, T.; Firdaus, K.; Adachi, S. *Phys. Rev. B* **2012**, *86*, 205103-1 – 25103-7.